A laser communication adaptive optics system as a testbed for extreme adaptive optics

Lewis C. Roberts, Gary Block, Santos Fregoso, Harrison Herzog, Seth R. Meeker, et al.

Lewis C. Roberts, Gary Block, Santos Fregoso, Harrison Herzog, Seth R. Meeker, Jennifer E. Roberts, Joshua Rodriguez, Jonathan Tesch, Tuan Truong, "A laser communication adaptive optics system as a testbed for extreme adaptive optics," Proc. SPIE 10703, Adaptive Optics Systems VI, 107031S (10 July 2018); doi: 10.1117/12.2314304

SPIE.

Event: SPIE Astronomical Telescopes + Instrumentation, 2018, Austin, Texas, United States

A Laser Communication Adaptive Optics System as a Testbed for Extreme Adaptive Optics

Lewis C. Roberts Jr.[a], Gary Block[a], Santos Fregoso [a], Harrison Herzog[a], Seth R. Meeker[a], Jennifer E. Roberts[a], Joshua Rodriguez[a], Jonathan Tesch[a], and Tuan Truong[a]

[a]Jet Propulsion Laboratory, California Institute of Technology, 4800 Oak Grove Dr, Pasadena CA 91109, USA

ABSTRACT

The Integrated Optical System (IOS) is an extreme adaptive optics system designed for NASA's Laser Communication Relay Demonstration mission. There is a great deal of overlap between the requirements for laser communication AO and high-contrast exoplanet imaging AO systems. Both require very high Strehl ratios with narrow fields of view. This overlap allows the IOS to serve as a testbed and technology demonstrator for astronomical extreme adaptive optics systems.

There are several example technologies from the IOS that are already making the transition to astronomical AO systems. The first is that the real time controller based on Direct Memory Access transfer between the WFS camera link frame-grabber and a DSP board is being reused on the upgrade to PALM-3000 AO system at Palomar Observatory. This enables the system to minimize latency by bypassing the CPU and its inherent timing jitter. Technologies like this will be crucial to enabling high contrast imaging on the next generation of extremely large telescopes. In addition, the IOS measures Fried's parameter from wavefraont measures in near real time. This technology has already been deployed to PALM-3000. The main function of Laser Communication AO systems is to couple the incoming light into single mode fiber. This is the same configuration that will be used by AO coupled radial velocity spectrographs.

The adaptive optics system is a woofer/tweeter design, with one deformable mirror correcting for low spatial frequencies with large amplitude and a second deformable mirror correcting for high spatial frequencies with small amplitude. The system uses a Shack-Hartmann wavefront sensor. The system has achieved first light and is undergoing commissioning. We will present an overview of the system design and initial performance.

Keywords: Laser Communication, Adaptive Optics

1. INTRODUCTION

The Laser Communications Relay Demonstration (LCRD) project is NASA's multi-year demonstration of laser communication between multiple ground stations and a geosynchronous satellite. LCRD will provide high data rate optical communications, demonstrating that optical communications can meet NASAs growing need for higher data rates while also enabling lower power, lower mass communications systems on spacecraft. In addition, LCRDs architecture will serve as a developmental test bed for additional methods, including symbol coding, ranging, link layer protocols, and network layer protocols.[1] LCRD will serve as a test bed for future NASA missions including the development of a future Advanced Telecommunications and Data Relay Satellite Service.[2] The mission is led by Goddard Space Flight Center (GSFC) with the participation of Massachusetts Institute of TechnologyLincoln Laboratory (MITLL), and Jet Propulsion Laboratory (JPL).

The LCRD space terminal will be a hosted payload on the U.S. Air Force's Space Test Program Satellite-6 (STPSat-6)[3] in geosynchronous orbit. The space terminal is capable of simultaneously communicating with two ground stations. There are currently two optical ground stations. Optical Ground station 1 (OGS1) is located at JPL's Table Mountain Observatory in Wrightwood California.[4] It will use the 1-m Optical Communication Telescope Laboratory (OCTL) telescope.[5] Optical Ground station 2 (OGS2) will be located at the U.S. Air

Further author information: (Send correspondence to L.C.R.)
L.C.R.: E-mail: lewis.c.roberts@jpl.nasa.gov

Adaptive Optics Systems VI, edited by Laird M. Close, Laura Schreiber, Dirk Schmidt, Proc. of SPIE Vol. 10703, 107031S · © 2018 SPIE
CCC code: 0277-786X/18/$18 · doi: 10.1117/12.2314304

Forces Maui Optical and Supercomputing on top of Haleakala in Maui, Hawaii. It will will use a 0.6m receive telescope and a 0.15m transmit telescope.[6]

Optical Ground station 1 (OGS1) consists of multiple systems including the existing OCTL telescope, the communication and beacon lasers, the monitor and control system, laser safety and the Integrated Optical System (IOS), which is the subject of this paper. The IOS system has two major functions. The first is to relay light from the beacon and communication lasers to the telescope. The second function is to relay the received light from the telescope to the ground modem's single mode fiber. Coupling the light into the single mode fiber requires an adaptive optics system that produces high Strehl ratios.

Section 2 discusses the opto-mechanical system, while the software is described in Section 3. Section 4 describes how elements of the IOS can be used on or benefit astronomical AO systems. Finally the future of the AO system is discussed in Section 5.

2. RECEIVE SYSTEM

A number of requirements were levied on the IOS. Of those, three drive the complexity of the system. As the exact location of the host satellite was unknown at the start of the design process, the IOS is required to operate at elevation angles as low as 20°. Recently the satellite location was specified to be between 112-120° with a target of 107°. This puts it at an elevation angle of 50° for OGS1. The system is also required to work at the median seeing conditions at the Table Mountain, or a Fried's parameter of 5.2 cm measured at zenith at a wavelength of 500 nm. Finally the system was required to work day or night. Under these conditions the IOS is required to produce a coupling efficiency of 55%, which translates to a Strehl ratio of roughly 70%. The nominal received power levels will be 125nW/m^2 at the front of the IOS.

AO is a technique where a deformable mirror is used to correct aberrations in the wavefront. These aberrations are sensed by a wavefront sensor (WFS). There are multiple types of wavefront sensors, each with its own advantages and disadvantages.

We chose a Shack-Hartmann sensor in a Fried geometry for the WFS. Most astronomical AO systems make their wavefront sensing measurements at one wavelength, and correct at another wavelength. For laser communication, where there is only a single incoming wavelength, we have to divert part of the incoming light to the WFS. The IOS has a baseline diversion of 20%, but we are reevaluating that based on the newly determined location of the satellite. The LCRD downlink wavelength is 1545 nm. The speed of the WFS measurement is critical for the AO system to keep up with the rapidly changing atmospheric turbulence conditions at the required 20° elevation and nominal r_0 of 5.2 cm. Our models have shown that we need to have frame rates on the order of 10 kHz to achieve our desired level of performance in the specified atmospheric conditions. The WFS camera is an off the shelf Xenics Cheetah InGaAs camera. Each lenslet in the WFS will illuminate an array of 2×2 detectors on the WFS focal plane array.

We carried out a trade study on the number of actuators across the primary. A higher actuator density will reduce the wavefront fitting error, but the WFS will have fewer photons per lenslet to make the wavefront measurements, which will increase the wavefront measurement error. In the end, we decided that 28 actuators across the primary mirror diameter would produce the best trade off between fitting error and measurement error. This lead us to the choice to use a Boston Micromachines 32×32 actuator Kilo-C MEMS DM[7] with a continuous facesheet. This DM only has an actuator stroke of 1.5 μm, which in turn drives us to use a woofer/tweeter design using the Boston Micromachines 12×12 actuator 3.5 μm stroke Multi-DM in addition to the Kilo DM. Our current stroke budget shows that we need 3.1 μm of stroke for the required 20° elevation angle, which gives us 12% margin. For the actual elevation angle of 50°, we will have 23% margin. In a woofer/tweeter design, a Low Order DM (LODM) corrects low spatial frequencies and large amplitude aberrations, while a High Order DM (HODM) corrects high spatial frequencies and small amplitude aberrations. MEMS DM have two advantages over conventional DMs. They are much smaller in diameter, on the order of 1 cm, which allows the rest of the optical train to be smaller. This reduces the cost of the optical train. Also the DMs themselves cost less than conventional DMs.

The IOS will be located in the coudé room of the OCTL facility. This room allows for multiple experiments to be set up simultaneously; a flat mirror on a rotation stage directs the optical beam to the desired experiment. The

IOS will be located on a standard optical bench, and will be isolated from the room atmospheric turbulence with an enclosure that also blocks stray laser light from leaving the optical bench. The IOS components are mounted on four separate breadboards which are mounted on the optical bench, which is shown in Figure 1 Having the IOS mounted on separate breadboards facilitates moving the system from the development laboratory to the telescope. Also, the WFS and a portion of the transmit system are aligned separately.

In the following description, we trace the light going through the receive system as it comes from the telescope. The description starts at the Transmit/Receive Dichroic. In Figure 1, this is where the red line intersects the blue line. First the beam hits acquisition camera pickoff. A portion of the light gets diverted to a camera that images the uncompensated light. This is used to acquire the target and then to measure the Fried's parameter at 1 Hz. Next the light encounters the first of five off-axis parabola (OAP1) mirrors, which forms a pupil on the fast steering mirror (FSM). Then the downlink beam encounters OAP2 and OAP3, which form a second pupil on the HODM. The beam then encounters OAP4 and OAP5 which form a third pupil on the LODM. The next optic is a pair of filters that block any back scattering from the uplink beam from entering the downstream sensors. The wavefront sensor picks off 10% of the light with a beamsplitter. Another 10% of the light is picked off for the scoring camera. Then the light is coupled into the single mode fiber that goes to the ground terminal. The AO system takes up most of a fairly large optical bench. Long focal length OAPs were used to ease the alignment; for other applications the system could be made much more compact.

The system also has an atmospheric turbulence simulator (ATS). A mirror can be slid into the beam path to inject light from the ATS into the AO system. The beam has the same optical properties as the downlink from the telescope and forms pupil images at the same locations. The ATS consists of two spinning phase plates with computer controlled rotation rates to simulate a variety of turbulence conditions.[8] The ATS will allow the IOS AO system to be tested in the lab over a wide variety of atmospheric conditions. This will improve the quality of the AO system, so that it will be farther down the development path when it gets to the telescope. It can also be left on for several days to help find bugs that will impair operations. Doing this in the laboratory is much more efficient than doing it at the telescope saving time and labor costs. The telescope is a limited resource and can be closed due to inclement weather. Also, specific atmospheric conditions are not available on demand, but depend on the whim of nature. During operations the ATS will be used for regression testing when the system is started up. The performance on these standardized tests will allow us to track IOS performance over the course of the mission and hopefully detect failing components before they totally fail.

As mentioned above, a portion of the downlink beam is diverted to the scoring camera. The scoring camera produces an image of the compensated downlink beam. This is used to judge the quality of compensation by measuring the Strehl ratio. The IOS also receives a measurement of the received power in the modem, but that is slightly delayed and is also not available before the launch of the space terminal. The scoring camera is also used to measure the non-common path aberrations in the system using the Modified Gerchberg-Saxton (MGS) algorithm.[9] The aberrations, which are not sensed by the WFS, can then be corrected by the DMs leading to improved image quality.

3. SOFTWARE ARCHITECTURE

The IOS software is based on the PALM-3000 software design.[10] Where functionally possible, existing PALM-3000 software was reused. We estimate that we have reused approximately 50% of the PALM-3000 code; this was a great time saver. As the IOS software is effectively a second generation version of the PALM-3000 code; this provides opportunities to incorporate lessons learned and to improve on the existing code.

The system design is divided into four main components: a command/automation server, a device driver server, the real-time control component, and the graphical user interface running on a computer in the operators room. The publish/subscribe communication method is used to transfer messages between components, a particularly effective method for systems with components running in physically separate locations. The real-time component uses a Digital Signal Processor (DSP) board with eight on-board DSP chips. We use direct memory access (DMA) to get data from the frame grabber directly to the DSP board enabling us to achieve the required frame rates. All published data is written to the database in the form of commands, status messages, and telemetry data. A separate component acts as the interface to the database; a slightly enhanced version of the

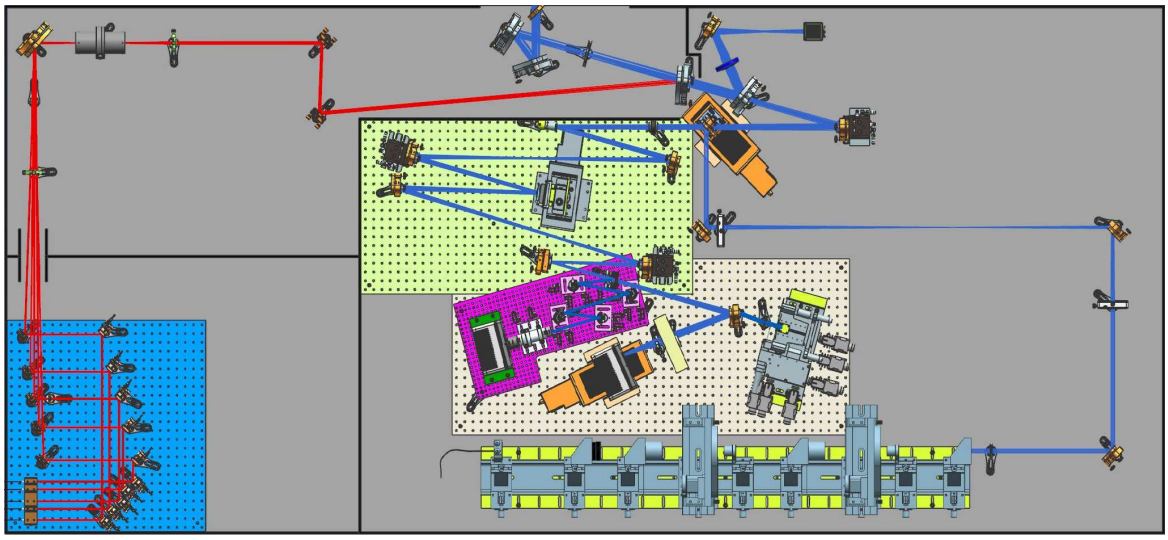

Figure 1. The IOS opto-mechanical layout. The transmit arm is marked in red, and the AO arm in blue. The WFS is mounted on the purple breadboard. The remaining components in the AO arm are divided between the tan and green breadboards. Much of the transmit system is mounted on the blue bread board on the left. The Atmospheric Turbulence Simulator (ATS) is at the bottom of the layout.

Berkeley DB database engine. A solid state drive in the IOS control computer is capable of capturing all of telemetry data types at the highest possible log rates. This will enable us to analyze performance during testing and operations.

Graphic Processor Units (GPU) based systems have become the standard for low latency AO real-time control systems.[11,12] While GPU systems are able to meet latency requirements of many instruments in operation today, they are limited in their processing capability by two factors: the lack of GPU support for application-level direct access to PCI Express and the absence of frame grabbers with application-tuned direct memory access (DMA) transfer size capability. IOS has solved this problem by using a multi-DSP based real-time control system that leverages the PCI Express multicast capability and a DMA-tuned frame grabber.

As the WFS takes an image it is captured by the frame grabber. From the frame grabber, the image is read out row by row. When there are two rows of data available, it gets shipped to the DSP board. Each of the eight DSP chips on the board contains eight cores. Each of the 64 cores measures the centroids of all the lenslets, but each core is assigned specific DM Actuators to compute the commands for. When the commands are computed, the DMA controller on each DSP chip transfers the DM commands to the appropriate DM via DMA. All of the above steps are done via DMA, which bypasses the central processing unit (CPU) and eliminates the CPU timing jitter. This enables us to deliver processing rates in excess of 20 kHz and a latency in the single-digit microsecond range for 56×64 pixel frames.

The IOS GUI was written in javascript and is run on any internet browser. It can be run on any computer that is on the same network as the IOS real-time control computer and can even be run from a smart phone. If more than one GUI is started, the first has operational control of the system, while subsequent versions of the GUI are allowed to monitor performance, but not allowed to change parameters.

4. APPLICATIONS TO ASTRONOMICAL AO

4.1 Real Time Controller

As mentioned above, the IOS has created the next generation of the real time control (RTC) software used on PALAO[13] and PALM-3000[11] AO systems. Each generation of the RTC has expanded capabilities and the ability to operate at faster speeds with more actuators. While the software is not reused, the experience of writing the RTC has enabled each succcessive generation. The JPL AO team is currently updating PALM-3000 with a

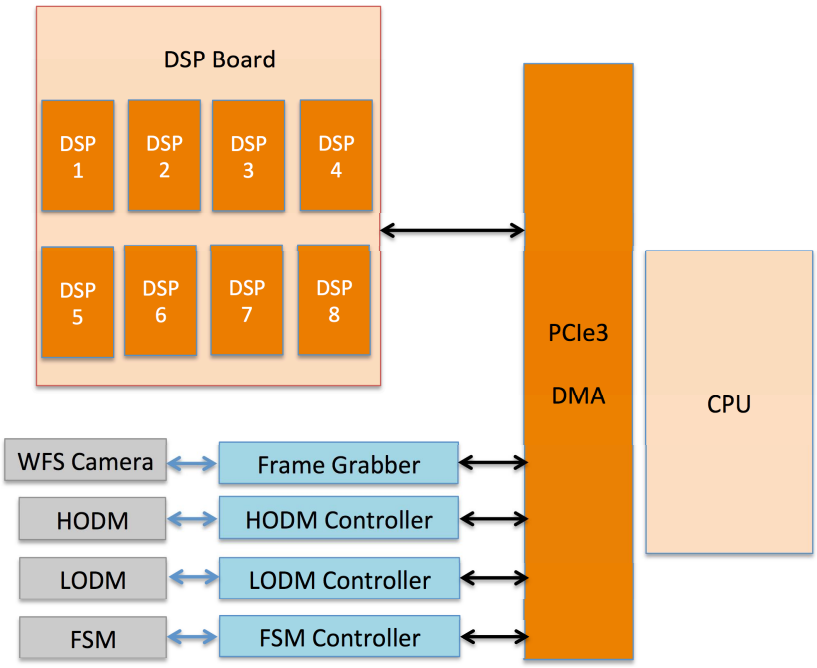

Figure 2. Data are exchanged between the frame grabber, the DSP card and the active mirror elements via DMA, without going through the CPU, which would add timing jitter and increase the control loop latency, leading to degraded performance.

new WFS based on an OCAM2 camera. In addition the updated PALM-3000 RTC is taking advantage of the experience gained in developing the IOS RTC and has switched from GPU to DSPs. This will replace the 10 computers running GPU boards mounted to the side of the telescope with a single computer and an expansion box housing four DSP cards.

4.2 r_0 Measurement

An understanding of r_0 is useful for understanding the performance of an AO system. Seeing measurements normally come from differential image motion monitors (DIMMS), which are located at different locations than the AO system's telescope and are usually constrained to take measurements once every few minutes. When the seeing measurements are taken in a separate facility, it limits the ability to understand dome seeing. To mitigate these issues, we have developed a method for measuring r_0 from WFS data using the slope discrepancy.[14]

The slope discrepancy is the difference between the measured slopes and the slopes computed from a reconstructed wavefront reconstructed from the measured slopes.[15] The difference is caused by noise, turbulence and branch points. Branch points are not considered to be an issue for the IOS since we are observing in conditions with Rytov values less than 0.2. The noise is estimated from the measurements and this allows the technique to be used to measure the r_0. The slope discrepancy is a useful measure because both result is the same if the AO system is operating open loop or closed loop.

Another benefit of the slope discrepancy is that a frame of WFS produces many measurements of the slope discrepancy which reduces the noise and increases the accuracy of the measurement. This allows a measurement of r_0 to be computed from only a few WFS frames increasing the measurement rate. This compares to DIMMs which usually collect measurements every few minutes.

We developed this technique for the IOS, but deployed it to Palomar on the PALM-3000 AO system as a risk reduction effort. On 17 June 2016 UT, we collected data with the PALM-3000 AO system. The frame rate of the saved WFS data was 968 fps and we collected 9 seconds of data. For that night, we also had measurements for of r_0 from the Palomar DIMM at a much lower frame rate. The r_0 values show general agreement. When the IOS is operational at the observatory, we plan to collect additional data and compare it with the DIMM at Table Mountain.

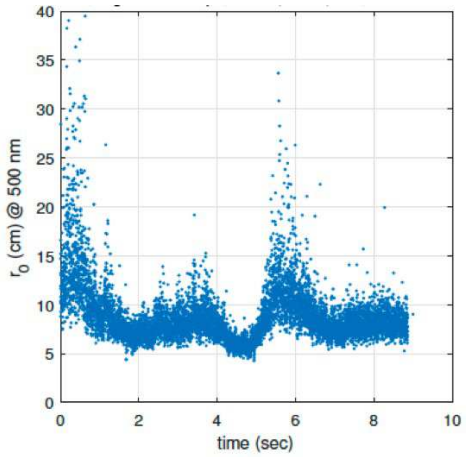

Figure 3. A sample time series of r_0 taken at Palomar with the PALM-3000 AO system.

4.3 Multi-channel Adaptive Control

Recent demonstrations have shown improved wavefront correction using optimal controllers, such as linear-quadratic regulators, which mitigate AO system latency and reduce broadband turbulence. These approaches typically include an offline procedure to identify models of the AO plant dynamics and external disturbances. However, high contrast imaging requires continuous closed-loop operation of many hours, and optical communication AO systems operate for long periods of time (for systems in geosynchronous orbit), or under rapidly changing conditions (for systems in low earth orbit). Both will benefit from a method for autonomously tracking non-stationary turbulence statistics.

Efforts are underway to implement a prototype adaptive control algorithm within the IOS real-time software architecture. The prototype is based on the receding horizon adaptive controller presented in Tesch et al.[16] and Tsuchiya et al.,[17] and uses a recursive least-squares lattice filter to implicitly track time-varying disturbance statistics. The controller is fully multichannel, providing joint adaptation over modes that may be spatially or temporally correlated.

Figure 4 shows early simulation results comparing the performance of the receding horizon controller against a well-tuned integrator for a single spatial mode. The simulation was driven using open-loop disturbances collected from the IOS Atmospheric Turbulence Simulator, with the turbulence strength gradually increasing around t=6.5 sec. In this example the adaptive controller outperforms the integrator, and adapts to the new disturbance statistics when the turbulence strength is increased. The power spectrum of the adaptive control residuals are nearly white for the duration of the simulation, indicating that the controller fully exploits correlations in the disturbance statistics.

We are currently implementing and testing multi-channel adaptive control on the IOS. With this control scheme, the AO system adapts to changing conditions and adjusts the loop behavior to maximize the system performance. We carried out simulations of our controller based on data taken from the IOS with the ATS acting as the disturbance. The results of the simulation are shown in Figure 4.

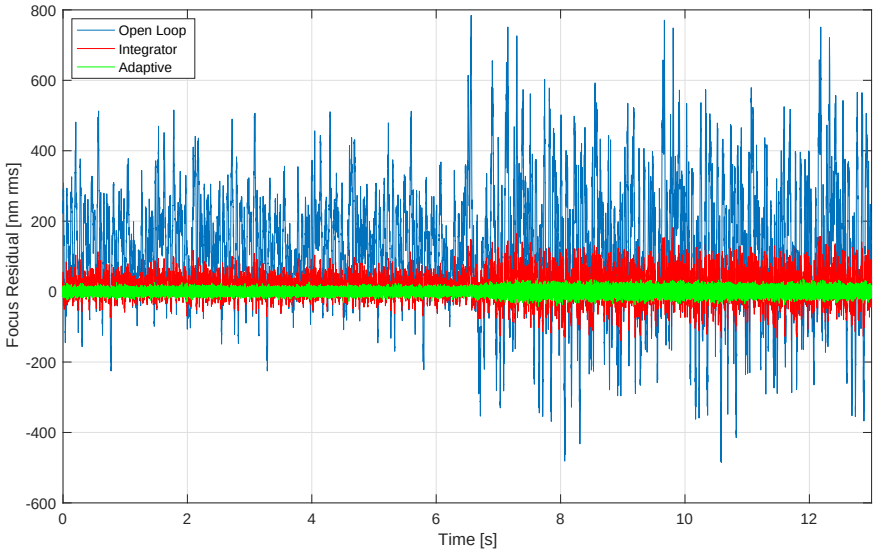

Figure 4. Focus error residuals from a simulation comparing a classical integrator with a receding-horizon adaptive controller. The simulation used a turbulence sequence recorded from the IOS Atmospheric Turbulence Simulator with wind speed and disturbance strength increasing at approximately t=6.5 sec.

4.4 PSF Behavior Studies

The IOS score camera is capable of taking frames at 400 Hz and subframes at kiloHertz rates. This will enable us to study the structure and dynamics of the PSF under a variety of turbulence conditions.[18] Several exoplanet detection algorithms have been proposed that use the differences in statistics between between speckles and faint exoplanets.[19] We are planning on carrying out a series of experiments that will measure the distribution of speckles.

4.5 Fiber Coupling

The IOS couples the light into a single mode fiber that is part of the communication modem.[20] We will be measuring the non-common path aberrations between our scoring camera and the WFS with the MGS algorithm. That is the normal approach for an AO system with a science camera, but in our case the fiber is our final "science" instrument. Since the modem only reports back received power we can not use it for MGS. Instead we plan on using Zernike tuning to remove any residual aberrations.

We are also concerned about mechanical drift between the fiber and AO beam due to diurnal thermal changes. We expect these to be small because the coudé room of the telescope is temperature controlled, but we want to be able to compensate for any that we do experience. To remove these aberrations we have a 5-axis fiber positioner. We plan on using the measured signal in the fiber as a metric. If the received power falls below a threshold, we will move the fiber tip a small amount in the positive direction and a matching amount in the negative direction. We will then compute a new position for the fiber based using a 2-step compare procedure used by on the Gemini Planet Imager calibration system. This will be done for each axis. If this algorithm is not sufficient, we will try more complex algorithms. The lessons and techniques used by the IOS to maximize power in the fiber will be of use to AO fiber fed spectrograph such as iLocator[21] and high-dispersion coronagraphy.[22]

5. THE FUTURE

The IOS has been fully integrated in the laboratory. We have closed the loop and are diagnosing the performance. One of the next steps we have to carry out is the removal of non-common path aberrations using the MGS algorithm. Later this summer, we will take it to the telescope. After realigning the system, we will begin a series

of regression tests to confirm that the system is performing the same as it did in the laboratory. After that we will begin a series of on sky tests to further optimize the system. During 2019, we expect to carry out many of the PSF studies and other experiments. The LCRD mission's space terminal is currently scheduled to launch in October of 2019. The spacecraft will undergo system checkout when it reaches orbit; we expect to begin laser communication operations in early 2020.

ACKNOWLEDGMENTS

The research was carried out at the Jet Propulsion Laboratory, California Institute of Technology, under a contract with the National Aeronautics and Space Administration (NASA).

REFERENCES

[1] E. Luzhansky, B. Edwards, D. Israel, D. Cornwell, J. Staren, N. Cummings, T. Roberts, and R. Patschke, "Overview and status of the Laser Communication Relay Demonstration," in *Free-Space Laser Communication and Atmospheric Propagation XXVIII*, H. Hemmati and D. M. Boroson, eds., *Proc. SPIE* **9739**, pp. 97390C–1, 2016.

[2] B. L. Edwards, D. Israel, K. Wilson, J. Moores, and A. Fletcher, "Overview of the Laser Communications Relay Demonstration project," *Proc. of the International Conference of Space Operations* , p. 1261897, 2011.

[3] B. M. Braun, S. M. Sims, J. McLeroy, and B. Brining, "Breaking (space) barriers for 50 years: The past, present, and future of the dod space test program," in *Year In Review*, *Proceedings of the AIAA/USU Conference on Small Satellites*, pp. SSC17–X–02, 2017.

[4] W. T. Roberts, D. Antsos, A. Croonquist, S. Piazzolla, L. C. Roberts, V. Garkanian, T. Trinh, M. W. Wright, R. Rogalin, J. Wu, and L. Clare, "Overview of Optical Ground Station 1 of the NASA Space Communications and Navigation Program," in *Free-Space Laser Communication and Atmospheric Propagation XXVIII*, H. Hemmati and D. M. Boroson, eds., *Proc. SPIE* **9739**, pp. 97390B–1, 2016.

[5] K. Wilson, M. Britcliffe, and N. Golshan, "Progress in design and construction of the Optical Communications Telescope Laboratory (OCTL)," in *Free-Space Laser Communication Technologies XII*, G. M. and, ed., *Proc. SPIE* **3932**, pp. 112–116, 2000.

[6] B. L. Edwards, D. J. Israel, and S. K. Vithlani, "Latest changes to NASA's laser communications relay demonstration project," in *Free-Space Laser Communication and Atmospheric Propagation XXX*, H. Hemmati and D. M. Boroson, eds., *Proc. SPIE* **10524**, p. 105240P, 2018.

[7] T. Bifano, "Shaping light: MOEMS deformable mirrors for microscopes and telescopes," *Proc. SPIE* **7595**, p. 759502, 2010.

[8] S. Mantravadi, T. Rhoadarmer, and R. Glas, "Simple laboratory system for generating well-controlled atmospheric-like turbulence," in *Advanced Wavefront Control: Methods, Devices, and Applications II*, J. Gonglewski, M. T. Gruneisen, and M. K. Giles, eds., *Proc. SPIE* **5553**, pp. 290–300, 2004.

[9] R. Burruss, E. Serabyn, D. Mawet, J. Roberts, J. Hickey, K. Rykoski, S. Bikkannavar, and J. Crepp, "Demonstration of on sky contrast improvement using the modified Gerchberg-Saxton algorithm at the Palomar Observatory," in *Free-Space Laser Communication and Atmospheric Propagation XXVIII*, B. Ellerbroek, M. Hart, N. Hubin, and P. L. Wizinowich, eds., *Proc. SPIE* **7736**, p. 77365X, 2010.

[10] T. N. Truong, A. H. Bouchez, R. S. Burruss, R. G. Dekany, S. R. Guiwits, J. E. Roberts, J. C. Shelton, and M. Troy, "Design and implementation of the PALM-3000 real-time control system," *Proc. SPIE* **8447**, p. 844702F, 2012.

[11] R. Dekany, J. Roberts, R. Burruss, A. Bouchez, T. Truong, C. Baranec, S. Guiwits, D. Hale, J. Angione, T. Trinh, J. Z. , J. C. Shelton, D. Palmer, J. Henning, E. Croner, M. Troy, D. McKenna, J. Tesch, S. Hildebrandt, and J. Milburn, "PALM-3000: Exoplanet adaptive optics for the 5 m Hale telescope," *ApJ* **776**, p. 130, 2013.

[12] N. W. Spellmeyer, C. A. Browne, D. O. Caplan, J. J. Carney, M. L. Chavez, A. S. Fletcher, J. J. Fitzgerald, R. D. Kaminsky, G. Lund, S. A. Hamilton, R. J. Magliocco, O. V. Mikulina, R. J. Murphy, H. G. Rao, M. S. Scheinbart, M. M. Seaver, and J. P. Wang, "A multi-rate dpsk modem for free-space laser communications," *Proc. SPIE* **8971**, p. 89710J, 2014.

[13] M.Troy, R. G. Dekany, G. L. Brack, B. R. Oppenheimer, E. E. Bloemhof, T. Trinh, F. G. Dekens, F. Shi, T. L. Hayward, and B. R. Brandl, "Palomar adaptive optics project: status and performance," *Proc. SPIE* **4007**, pp. 31–40, 2000.

[14] T. J. Brennan and D. C. Mann, "Estimation of optical turbulence characteristics from Shack Hartmann wavefront sensor measurements," *Proc. SPIE* **7816**, p. 781602, 2010.

[15] G. A. Tyler, "Reconstruction and assessment of the least-squares and slope discrepancy components of the phase," *J. Opt. Soc. Amer. A.* **17**, pp. 1828–1839, 2000.

[16] J. Tesch, S. Gibson, and M. Verhaegen, "Receding-horizon adaptive control of aero-optical wavefronts," *Opt. Eng* **52**, p. 071406, 2013.

[17] N. Tsuchiya, S. Gibson, T.-C. Tsao, and M. Verhaegen, "Receding-horizon adaptive control of laser beam jitter," *IEEE/ASME Trans. Mechatronics* **21**, pp. 227–237, 2015.

[18] N. Yaitskova, M. Esselborn, and S. Gladysz, "Statistical moments of the strehl ratio," in *Adaptive Optics Systems III*, B. L. Ellerbroek, E. Marchetti, and J.-P. Véran, eds., *Proc. SPIE* **8447**, p. 84475Y, 2012.

[19] S. Gladysz and N. Yaitskova, "Temporal variability and statistics of the strehl ratio in adaptive-optics images," *Proc. SPIE* **7387**, p. 73870Z, 2010.

[20] A. Sevin, D. Perret, D. Gratadour, M. Lainé, J. Brulé, and B. L. Ruyet, "Enabling technologies for GPU driven adaptive optics real-time control," *Proc. SPIE* **9148**, p. 91482G, 2014.

[21] J. R. Crepp and et al., "iLocater: a diffraction-limited doppler spectrometer for the Large Binocular Telescope," *Proc. SPIE* **9908**, p. 990819, 2016.

[22] N. K. Y. Xin, D. Mawet, G. Ruane, J.-R. Delorme, W. Xuan, D. Echeverri, M. Randolph, J. Fucik, J. K. Wallace, J. Wang, G. Vasisht, R. Dekany, B. Mennesson, E. Choquet, and E. S. and, "Utilizing active single-mode fiber injection for speckle nulling in exoplanet characterization," *Proc.* **10400**, p. 104000Y, 2015.